Ground and excited-state fermions in a one-dimensional double-well: Exact and density-functional solutions

R. J. Magyar*
The National Institute of Standards and Technology, 100 Bureau Drive, MS 8380, Gaithersburg, Maryland 20899, USA
(Received 24 August 2007; revised manuscript received 29 March 2009; published 26 May 2009)

Two of the most popular quantum-mechanical models of interacting fermions are compared to each other and to potentially exact solutions for a pair of contact-interacting fermions trapped in a one-dimensional (1D) double-well potential, a model of atoms in a quasi-1D optical lattice, or electrons of a hydrogen molecule in a strong magnetic field. An exact few-body Hamiltonian is solved numerically in momentum space yielding a highly correlated eigenspectrum. Additionally, approximate ground-state energies are obtained using both density-functional theory (DFT) functional and two-site Hubbard models. A 1D adiabatic local-density approximation kernel is constructed for use in time-dependent density-functional theory (TDDFT) and the resulting excited-state spectrum is compared to the exact and Hubbard results. DFT is shown to give accurate results for wells with small separations but fails to describe localization of opposite spin fermions to different sites. A *locally cognizant* density functional based on an effective local fermion number would provide a solution to this problem, and an approximate treatment presented here compares favorably to the exact and Hubbard results. The TDDFT excited-state spectrum is accurate in the small parameter regime with nonadiabatic effects accounting for any deviations. As expected, the ground-state Hubbard model outperforms DFT at large separations but breaks down at intermediate separations due to improper scaling to the united-atom limit. At strong coupling, both Hubbard and TDDFT methods fail to capture the appropriate energetics.

DOI: 10.1103/PhysRevB.79.195127 PACS number(s): 71.10.−w, 71.15.Mb, 31.15.E−

I. INTRODUCTION

One of the underlying challenges in computational physics, notably in density-functional theory, is the accurate and reliable treatment of many-body interactions in matter. The typical interaction type that most electrons in solids experience is the Coulomb interaction and this is a pernicious one owing to its long-ranged nature. Many of the difficulties in providing accurate numeric results for Coulomb-interacting systems are the results of the long range. It would be insightful and beneficial to the development of techniques that explicitly describe many-body systems if the Coulomb interaction were instead a more local version. One such replacement, the contact interaction, offers a powerful test case to probe specifically the many-body problem without long-range complications. This is particularly important in the analysis and formal improvement of practical methods of electronic structure theory such as Hubbard theories and density-functional ones. In this paper, we explore a simple model system of fermions that interact via a contact interaction. Remarkably, the interacting quantum problem is shown here to reduce to a solvable system of integral equations. Additionally, we extend developments in the density-functional modeling of contact-interacting systems to the time-dependent domain. This work has implications both for the formal development of density-functional theory and for the practical numeric analysis of quasi-one-dimensional (1D) systems.

Contact interactions can arise as a simplified form of three-dimensional (3D) interactions in highly confined quasi-1D systems, experimentally realizable in 1D optical lattices.[1–3] In these situations, the contact term is a reasonable approximation to the interaction when the ratio of the interaction strength to the transverse well width is large. An additional approximation made is that the wave-function, although still 3D, factors into transverse and longitudinal components with the interaction only affecting the longitudinal part. We consider only the nontrivial longitudinal part. Thus, the 3D interaction is replaced by a 1D one. Admittedly, a more realistic reduction of the 3D Coulomb problem to an effectively 1D one is widely debated and, here, we have chosen a particular form partially motivated by the advantages it offers computationally.

A major computational advantage of the δ-function interaction within the density-functional theory (DFT) is that the exchange and Hartree functionals are explicit functionals of the fermion density, a result implying that the local-density approximation (LDA) to exchange is self-interaction free. Thus, the functionals used for Hartree and exchange represent the exact-exchange formalism (EXX). This locality of EXX is not true for the long-ranged 3D Coulomb interaction and performing EXX in 3D is a significantly more complicated endeavor. For the full LDA in the 1D case, any inaccuracies are caused by the mismodeling of correlation. In 3D, the inaccuracies are mixed between exchange and correlation due to the long-ranged nature of the Coulomb potential. A notable example of a long-ranged correlation problem is the inability of the LDA to localize single electrons on distant sites. Hubbard theory, on the other hand, preserves this limit but sacrifices accuracy.

For these reasons and the clarifying simplicity of 1D models, the δ-function model for 1D fermions has been considered in several recent studies. In particular, the introduction of a local-density correlation functional has provided exceptionally accurate results for the ground state of finite systems such as the Diracium[4] and the 1D analog of Hooke's atom.[4,5] A modified parameterization of the LDA has been used to describe interacting fermions in harmonic confining

potentials.[5] A time-dependent Thomas-Fermi theory has been used to predict the excited-state properties of a many-fermion system but did not amount to the Kohn-Sham (KS) formulation of DFT.[6] More general problems involving this contact interaction also have been studied recently.[7–9]

In this paper, we investigate a two-site δ-function problem, the 1D quantum analog of the H_2 molecule[10] or a two-site optical lattice, hitherto referred to as 1D H_2. The author expounds a 1D contact-interacting time-dependent density-functional theory (TDDFT) and compares the results to the exact solutions and to the two-site Hubbard results. In order to accurately express the 1D adiabatic LDA kernel, it is found necessary to improve the existing parameterization of the result for the reference system to include higher-order terms at the low- and high-density limits. The resulting functional reproduces the previously known expansion terms reported in Refs. 4 and 5 but additionally includes a critically important high-density term needed to describe the adiabatic LDA kernel. The author develops a numeric scheme to obtain the exact bound-state spectrum for 1D H_2 from a set of 1D integral equations. The results are tested against a general form of the virial theorem. Numeric integration techniques are developed to handle the oscillatory nature of the integrand. In the stretched system, the author contrives a scheme to correct the long-range correlation self-interaction error. The results are compared to the well-known two-site Hubbard model that is expected to be accurate in the long-separation limit.

Throughout, we assume that our 1D fermions have the same mass as electrons and we use atomic units ($e^2=\hbar=m_e=1$) so that all energies are in Hartrees, all lengths in Bohr radii, and the coupling constant in Bohr-Hartree . A realistic correspondence between the interaction strength λ and the details of a trapping potential are given by Ref. 11. Here, the external potential and interaction strengths are arbitrarily chosen so that the total energies come out in the typical chemical range for the sake of physical intuition.

II. ONE-DIMENSION CONTACT-INTERACTING FERMIONS IN A DOUBLE WELL

In this section, we state the quantum-mechanical model of trapped 1D fermions. From the noninteracting case, we anticipate how the many-body wave functions are structured.

The 1D Hamiltonian for the particle pair in a double well is

$$\hat{H} = -\frac{1}{2}\sum_{i=1}^{2}\frac{d^2}{dx_i^2} + \lambda\delta(x_1 - x_2) - Z\sum_{i=1,\pm}^{2}\delta(x_i \pm a). \quad (1)$$

The terms from left to right are the kinetic term, the contact-interaction strength, and the trapping potential with a being half the interwell spacing. Z and λ are the relative strengths of the local and interaction potentials. i labels the fermion number and x_i is the position of the ith fermion. The lowest-energy eigenfunction or ground-state wave function is assumed to vanish infinitely far from the trapping potential.

TABLE I. The noninteracting many-particle bound states of the Hamiltonian Eq. (1). + stands for the *gerade* single-particle orbital with eigenvalue ϵ_+, and − stands for the *ungerade* single-particle orbital with eigenvalue ϵ_-.

State	Nonint. occ. orb. 1	Nonint. occ. orb. 2	Exchange space	Symmetry spin	Two-body energy
S_0	+	+	Symm.	Asymm.	$2\epsilon_+$
S_1	+	−	Symm.	Asymm.	$\epsilon_+ + \epsilon_-$
S_2	−	−	Symm.	Asymm.	$2\epsilon_-$
T_1	+	−	Asymm.	Symm.	$\epsilon_+ + \epsilon_-$

The noninteracting problem has two single-particle eigenvalues: $\epsilon_\pm = -k_\pm^2/2$ with $k_\pm = Z + 1/(2a)\text{Lambert}W[\pm 2aZ\exp(-2aZ)]$.[8,12] The "+" corresponds to the lower energy spatially symmetric (*gerade*) single-particle bonding state and the "−" corresponds to the antisymmetric (*ungerade*) single-particle antibonding state. The Lambert$W(y)$ function is the principle solution for x of $y = x\exp(x)$. The normalized single-particle wave functions are $\phi_\pm(x) = N_\pm[\exp(-k_\pm|x-a|) \pm \exp(-k_\pm|x+a|)]$, where x is a noninteracting particle's position and $N_\pm$ equals $1/\sqrt{\frac{2}{k_\pm} \pm (4a + \frac{2}{k_\pm})\exp(-2k_\pm a)}$. While a *gerade* ground-state exists for all values of aZ, the *ungerade* state only exists for $aZ > 1/2$. We refer to the large separation case as stretched H_2 and the small separation as crushed H_2 tending to the united-atom limit. Table I characterizes the various noninteracting two-particle states and defines what is meant by the term designations S_0, S_1, S_2, and T_1.

The virial theorem is important in practical applications where it is often used to verify numeric results. In its fundamental form, it states that $2\langle\hat{T}\rangle = \langle\hat{x}\frac{d}{dx}V(\hat{x})\rangle$. The expectation value denotes an average over spatial variables of the respective eigenfunction solutions of Eq. (1). The modified version, generated through integration by parts and typically used for the Coulomb interaction, is $2\langle\hat{T}\rangle = -\langle V(\hat{x})\rangle$ but does not hold true here due to the fixed location of the external potential. A careful integration by parts shows that a generalized version,

$$2\langle\hat{T}\rangle + \langle V(\hat{x})\rangle = -2a\int_{-\infty}^{\infty} dy\,\psi^*(a,y)\overline{d/da\,\psi(a,y)} + 2a\int_{-\infty}^{\infty} dy\,\psi^*(-a,y)\overline{d/da\,\psi(-a,y)}, \quad (2)$$

is valid for the ground state of the system. Note that we use y here for the spatial coordinate to avoid confusion with x_1 and x_2. $\overline{d/da\,\psi(a,y)}$ is the average of the right and left

derivatives with respect to the first argument. The interaction potential part needs no modification. A many-site version of Eq. (2) holds for multiple δ wells but has more terms on the right of the equal sign. The right-hand side of the general version vanishes for an isolated δ well and a periodic lattice of wells because in these cases the average derivative is null by symmetry and the form of the virial theorem, $2\langle\hat{T}\rangle=-\langle V(\hat{x})\rangle$, is justified.

In the interacting problem, there are only two deciding parameters, λ and a. The external potential strength can be scaled to unity leaving the energy in units of Z^2 times the atomic unit and length in units of $1/Z$ times the atomic unit. This leaves four regimes to consider. λ small and a large is the weakly interacting two-well solution. λ large and a small is the highly correlated double-well solution. For sufficiently small a, the wells merge to the united-atom limit. When λ and a are large, we have a system where long-range correlations can be important. Finally, λ small and a small is a regime where the interaction can be treated perturbatively and the well is almost a single well. Large a is the domain of validity of the Hubbard model.

This paper examines two of these regimes in detail: the small width double-well, $a=1$, and the large range hopping scale, $a=2$: both with $Z=1$. We note that in the former range, the separation between the wells is large enough to exceed the united atom limit yet still preserves the existence of at least two bound states. The latter case ($aZ=2$) is the regime where Hubbard theory is designed to be maximally valid. For the remainder of the paper, we assume that $Z=1$.

The two-site Hubbard will be compared to the more general density functional and exact solutions. The Hubbard model itself is important for the conceptual picture it provides and its role in the popular LDA+U method a hybrid electronic method combining LDA DFT and Hubbard approaches.[13,14] Furthermore, the Hubbard picture is designed to reproduce localization in the stretched limit; a property that is not matched in the LDA version of DFT. In the Hubbard approach, the Hamiltonian Eq. (1) is simplified to a site-occupation form.[15] The simplification is valid when the wave-function overlap between sites is small as is the case for $a=2$ but not $a=1$. The approximate Hamiltonian can be diagonalized exactly and relies on two parameters: t (the hopping term) and U (the on-site repulsion).

To find t, the hopping term, we consider linear combinations of the noninteracting single-particle orbitals that give left and right localized fermions: $\phi_R(x)=[\phi_+(x)+\phi_-(x)]/\sqrt{2}$ and $\phi_L(x)=[\phi_+(x)-\phi_-(x)]/\sqrt{2}$. The hopping term is the projection, on one localized wave function, of the kinetic-energy operator acting on the other localized fermion wave function: $t=1/2\int dx\phi_R(x)\nabla^2\phi_L(x)=1/4(k_+^2-k_-^2)$. Note that we defined t to be positive. This definition is chosen to reproduce the proper long-range limit. Traditionally, the t term is fixed using nonorthogonal localized solutions. The difference is negligible in the large separation limit. For the small separation limit, our definition of t gives a different result than the traditional hopping term. This is because the ϕ_- state is no longer bound for small a, and consequently, the maximally *localized* solutions are not really localized to any one site. Curiously, the convention used here more accurately describes the energy in the noninteracting case at small separations than the traditional definition.

The Hubbard Hamiltonian can be exactly diagonalized and has eigenvalues $E_{S_0}=2\epsilon+\frac{U}{2}-\frac{1}{2}\sqrt{16t^2+U^2}$, $E_{S_1}=2\epsilon+U$, and $E_{S_2}=2\epsilon+\frac{U}{2}+\frac{1}{2}\sqrt{16t^2+U^2}$. Physically, the first-excited singlet state at large separation, a, corresponds to two fermions localized on one site. This is the Diracium system and a distant empty site. If we make a correspondence between the Hubbard energy of S_1 and the total energy of Diracium, U can be expressed as a function of λ. The total energy for S_1 is written $E=2\epsilon+U$, with $\epsilon<0$. The allowable range for U from Diracium is 0 to $-\epsilon$. Above this limit, at λ_{crit}, $U_{\text{crit}}^{\infty}=-\epsilon$ and the single well no longer binds two fermions. We match the Hubbard U value to give exact results given in Refs. 4 and 16. For example, a U of 0.354 gives the correct energy for Diracium with $\lambda=1$ and $Z=1$. For numerical convenience, we parameterize the interaction energy versus λ when $Z=1$: $U(\lambda)\approx 0.500\lambda-0.163\lambda^2+0.017\lambda^3+\mathcal{O}(\lambda^4)$, valid for $\lambda<\lambda_{\text{crit}}$ with a max error of about 0.5%.

Despite scaling problems, the Hubbard model is well trusted at large a because of its computational convenience and its facility with handling long-ranged ground-state correlations. LDA does not handle these correlations and even the exact solution method must be carefully formulated in this limit.

III. TIME-DEPENDENT DENSITY-FUNCTIONAL THEORY

In this section we generalize work done by us and others in ground-state density-functional theory to the time-dependent case. This extension requires several improvements upon the ground-state theory. There are four main results of this section: (1) the discovery of the importance in TDDFT of the third term in the high-density correlation energy, (2) the creation of an improved correlation functional that properly describes this term, (3) the proposal of a local effective fermion measure based on KS orbitals, and (4) the introduction of a new correlation functional that can properly describe spatially separated systems. The results can be found in Eqs. (3), (5), (14), and (15), respectively.

A general approach to find the ground-state energy and fermion density of 1D H_2 is to use DFT. In ground-state DFT, the details of the external potential are kept, but the many-body interaction is transformed to an effective local potential derived from the exchange-correlation density functional.[17,18] Given the exact exchange-correlation functional, DFT would return the exact results for the total energy and density. In practice, this exchange-correlation contribution is approximated. An active area of research in the 3D case is to improve the accuracy and reliability of approximations to the exchange-correlation functional.

According to spin-density-functional theory,[17] the ground-state total energy is a functional of the particle density and the local magnetization. In this work, we make the assumption that an axis of magnetization is chosen and the local magnetization is given by $\zeta(x)=[n_\uparrow(x)-n_\downarrow(x)]/[n_\uparrow(x)+n_\downarrow(x)]$, where $n_\uparrow$ and $n_\downarrow$ are up- and down-spin densities projected on the magnetization axis. The total ground-state energy can then be decomposed as fol-

lows: $E[n,\zeta]=T_S[n,\zeta]+E_H[n]+E_{\mathrm{XC}}[n,\zeta]+\int dx v_{\mathrm{ext}}(x)n(x)$ in 1D, where $E_H[n]$ is the exactly known Hartree or classical density-density interaction contribution, $v_{\mathrm{ext}}(x)$ is the given inhomogeneous potential, $T_S[n,\zeta]$ is the exactly known kinetic energy of noninteracting fermions at a given density and local magnetization, and $E_{\mathrm{XC}}[n,\zeta]$ is the exchange-correlation energy. The solution for the problem of interest is found by studying the KS system, the noninteracting counterpart to the physical system.[18] The spin densities are obtained from the occupied KS orbitals, $\phi_{i,\sigma}(x)$ according to $n_\sigma(x)=\Sigma_{i,\mathrm{occ.}}|\phi_{i,\sigma}(x)|^2$.

In the contact 1D case, the Hartree and exchange terms, $E_{\mathrm{HX}}[n_\uparrow,n_\downarrow]=\lambda\int dx n_\uparrow(x)n_\downarrow(x)$, are known exactly and only the correlation energy functional must be approximated in practice. It is important to note that the Hartree and exchange functional for this contact interaction is self-interaction free, so in essence, the pure density functional already includes explicitly EXX. Many of the known practical limitations of 3D DFT can be addressed by applying EXX but in 3D, this is computationally demanding. The LDA functionals in this paper include the EXX formalism, so the analysis and results here will be useful in the next development stage of DFT where EXX-compatible correlation is considered in detail. In particular, since the interaction here is local, certain difficult-to-model long-range aspects of correlation will be isolated. For example, contact-interacting fermions will still exhibit spin-density waves and long-ranged entanglement: two problems extremely difficult to model using traditional density-functional methods.

The correlation energy functional is often modeled using the correlation energy of a solvable reference system of fermions. For the chosen 1D interaction, this is the Gaudin-Yang model solved exactly via the Bethe-Ansatz technique.[19–21] The correlation energy per particle of the uniform system, $\epsilon_C^{\mathrm{unif}}$, can then be parameterized as in Refs. 4 and 5 to reproduce the exact curve. The high-density expansion is

$$\epsilon_C(n)=-\lambda^2/24+\lambda^3\zeta(3)/(2\pi^4 n)-\lambda^4 0.000\,94/n^2+\mathcal{O}(\lambda^5/n^3), \tag{3}$$

where, $\zeta(3)$ is the Riemann zeta function evaluated at 3. See Appendix A for the calculation of the second term.

The low-density correlation energy is

$$\epsilon_C(n)=-\lambda n/4+n^2\pi^2/8-n^3 2\pi^2\log(2)/(3\lambda)+\mathcal{O}(n^4/\lambda^2). \tag{4}$$

The low-density limit can be understood by noting that the interaction is so strong that it mimics Fermi repulsion, so it must cancel the Hartree and exchange terms and add a kineticlike contribution to the energy. The third term is referred to in Refs. 7 and 22.

A modified parameterization of the correlation energy per particle as a (4,4) Padé is

$$\epsilon_C^{\mathrm{unif}}(n)=\frac{An^3+Bn^2+Cn}{Dn^3+En^2+Fn+1}, \tag{5}$$

with $A=-7.031\,951$, $B=-2.169\,922$, $C=-0.25$, $D=168.766\,814$, $E=77.069\,721$, and $F=13.614\,491$. This parameterization gives three terms in both the high- and low-density expansions of the correlation energy. The error is less than 0.5% error in the correlation energy per particle for all densities. We note the remarkable fact that parameters, A-F, are determined exactly with no approximate numerical fit. Details are given in the Appendix B.

The LDA correlation energy functional is an integral over local contributions of the reference system's correlation energy per particle times the fermions per unit volume,

$$E_C^{\mathrm{LDA}}[n,\zeta]=\int_{-\infty}^{\infty}dx n(x)\epsilon_C^{\mathrm{unif}}(n(x))f(\zeta(x)). \tag{6}$$

$f(\zeta)$ contains information about the local magnetization dependence. The exact high-density limit for $f(\zeta)$ can be obtained via diagrammatic perturbation theory (Appendix C) and is approximately $f(\zeta)\approx(1-\zeta^2)$ used here for all densities. The improved (4,4) Padé parameterization of the LDA correlation energy functional is used because the ones given in Refs. 4 and 5 do not accurately reproduce the high-density correlation kernel needed for TDDFT as we will explain later.

The DFT solution is obtained through a self-consistent solution of the Kohn-Sham equations using a modified version of the DFT code in Ref. 4. In this code, a Numerov integration scheme is combined with the shooting method to obtain solutions of the Kohn-Sham equations. The number of grid points is chosen to converge energies to within mHartree accuracy, and the output is checked against an analytic EXX solution given in Appendix D.

Time-dependent DFT allows the determination of the excited states. The exact excitations occur at the poles of the density response-function.[23,24] Finding the excited-state transition energies amounts to the solution of a generalized eigenvalue problem

$$\Omega_{ij\sigma,kl\tau}(\omega_{(I)})F_{(I),kl\tau}=\omega_{(I)}^2F_{(I),ij\sigma}, \tag{7}$$

with

$$\Omega_{ij\sigma,kl\tau}(\omega)=\delta_{\sigma\tau}\delta_{ik}\delta_{jl}(\epsilon_{j\sigma}-\epsilon_{i\sigma})^2+2K_{ij\sigma,kl\tau}(\omega)\times\sqrt{(f_{i\sigma}-f_{j\sigma})(\epsilon_{j\sigma}-\epsilon_{i\sigma})}\sqrt{(f_{k\tau}-f_{l\tau})(\epsilon_{l\tau}-\epsilon_{k\tau})}, \tag{8}$$

where $\epsilon_{i\sigma}$ is the KS eigenvalue of the ith KS orbital of spin σ. $f_{i\sigma}$ is 1 if the ith orbital of spin σ is occupied; otherwise, $f_{i\sigma}$ is 0. $\omega_{(I)}$ is the Ith excitation value sought. $K_{ij\sigma,kl\tau}(\omega)$ depends on the exchange-correlation kernel as follows:

$$K_{ij\sigma,kl\tau}(\omega)=\int_{-\infty}^{\infty}dxdx'\,\phi_{i\sigma}^*(x)\phi_{j\sigma}^*(x)f_{\mathrm{HXC},\sigma\tau}(x,x',\omega)\times\phi_{k\tau}(x')\phi_{l\tau}(x'). \tag{9}$$

In general, the matrix $K(\omega)$ depends on the energy, ω, of the solution, and this greatly complicates the solution of the general problem. However, the ω dependence is often ignored in what is called the adiabatic approximation.

The adiabatic LDA kernel can be derived from the second functional derivative of the time-independent LDA exchange-correlation functional. Hence,

$$f_{\mathrm{HXC}\sigma\tau}^{\mathrm{LDA}}(x,x',\omega) = \frac{\delta^2 E_{\mathrm{HXC}}^{\mathrm{LDA}}[n,\zeta]}{\delta n_\sigma(x)\,\delta n_\tau(x')} = \lambda\,\delta(x-x')(1-\delta_{\sigma\tau}) + \left(\frac{d^2\{n(x)\epsilon_C(n(x))\}}{d^2 n(x)} + 2\frac{\epsilon_C(n(x))}{n(x)}(1-2\delta_{\sigma\tau})\right)\delta(x-x') = f_{\mathrm{HX}\sigma\tau}^{\mathrm{EXX}}(x,x') + f_{C\sigma\tau}^{\mathrm{LDA}}(x,x'). \quad (10)$$

The kernel is split into two parts: a Hartree-exchange part ($f_{\mathrm{HX}\sigma\tau}^{\mathrm{EXX}}$) and a correlation part ($f_{C\sigma\tau}^{\mathrm{LDA}}$). The former is known exactly and the latter must be approximated. The result after the second equal sign is tailored specifically to the application in this manuscript assuming an unpolarized $\zeta=0$ system.

Now, we will explain why we need to have an accurate correlation energy per particle to third order in the high-density limit. The second derivative of the correlation energy density with respect to the density represents the heart of the adiabatic TDDFT approximation as it carries all the correlation effects beyond what is modeled in the KS orbitals. The correlation kernel is the second functional derivative of Eq. (6) with Eq. (5) plugged in explicitly. In the high-density limit, the first two terms of its second derivative vanish and only the third and higher terms remain. Therefore, in order to model the correlation kernel *at all* in the high-density limit, the third term must be included. For this reason, we had to replace the (3,3) forms with the (4,4) Padé given in this paper. In 3D, the situation is different as the logarithmic dependence on the density means that the second derivative is divergent and nonvanishing; however, any additional finite terms might be neglected and third-order nonlogarithmic terms might become important in certain common density ranges.

The 1D H_2 model at hand has at most two-bound KS orbitals, so we use the two-state single-pole approximation to TDDFT—first presented by Casida.[24] It is assumed that the contribution of any finite number of unbound orbitals to the response function is negligible due to box normalization. It is possible however, in the limit of extremely weakly bound orbitals, that this approximation is no longer valid. The solution of Eq. (8) within the two-state model is

$$\omega_S = \sqrt{(\epsilon_1-\epsilon_0)[(\epsilon_1-\epsilon_0)+2(K_{\uparrow\uparrow}+K_{\uparrow\downarrow})]} \quad (11)$$

for the singlet excitation and

$$\omega_T = \sqrt{(\epsilon_1-\epsilon_0)[(\epsilon_1-\epsilon_0)+2(K_{\uparrow\uparrow}-K_{\uparrow\downarrow})]} \quad (12)$$

for the triplet excitation. ϵ_0 corresponds to the lowest-energy *gerade* KS orbital eigenvalue and ϵ_1 corresponds to the *ungerade* excited KS orbital eigenvalue. We use ϵ_0 and ϵ_1 here to distinguish these values from the exact noninteracting eigenvalues ϵ_+ and ϵ_- even though the KS states are also characterized as *gerade* and *ungerade*. K is a 2×2 matrix in spin given by

$$K_{\sigma\tau} = \lambda(1-\delta_{\sigma\tau})\int_{-\infty}^{\infty} dx\,\phi_0^2(x)\phi_1^2(x) + \int_{-\infty}^{\infty}\int_{-\infty}^{\infty} dx dx'\,\phi_0(x)\phi_1(x) f_{C\sigma\tau}^{\mathrm{LDA}}(x,x',\omega)\phi_1(x')\phi_2(x'). \quad (13)$$

In Sec. V, we will directly compare the exact excited-state spectrum for Eq. (1) and the TDDFT spectrum.

DFT will likely fail for large separations, a, because the local treatment of correlation does not cancel the exchange and Hartree terms. This is the long-ranged self-correlation error, sometimes called the static correlation problem in DFT, and it exists even when the interaction is local. The net effect is that two well-separated fermions interact in the LDA while in a realistic system, the fermions would be entangled but otherwise noninteracting. For ground-state DFT, we suggest a simple scheme to model the long-range correlation and to cancel the self-correlation error in the stretched case. First, note that in the stretched situation, there is no problem in the polarized case since two fermions of the same spin do not interact via the contact interaction. In the unpolarized case when $\zeta=0$, opposite spin particles are likely to localize in different regions of space; the interaction energy will be much less than expected if they delocalized. In order for this to be captured, the correlation energy must exactly cancel the Hartree-exchange energy. This is achievable if $\epsilon_C(n)=-\lambda n/4$ when $\zeta=0$, the negative of the Hartree and exchange energy. The solution is then to obtain information from the density that fermions are in the *stretched* regime and to apply long-ranged correlation in this case. A previous attempt at describing this long-ranged correlation used the pair density function with some success.[25] Another way this can be achieved is by relying on the KS orbitals and defining the dimensionless and unitary parameter,

$$\tau(x) = \frac{\sum_{\mathrm{occ}} |\phi_{i,\sigma}|^4(x)}{\left(\sum_{\mathrm{occ}} |\phi_{i,\sigma}|^2(x)\right)^2}, \quad (14)$$

where $\phi_{i,\sigma}$ represents the ith KS spin-orbital and the sum is over i and σ. If the fermions are isolated as in the case of a one fermion system, $\tau(x)=1$; otherwise, $\tau(x)<1$. For a two-fermion system such as Diracium, $\tau(x)=1/2$ and $\tau(x)=0$ for the uniform-reference system. Physically, τ can be thought of as a measure of the inverse number of fermions that are locally relevant and, in this way, transcends the definition given here. Unitary τ implies that a certain region of space is occupied by only one fermion and so many-body effects are trivially unimportant. As τ gets smaller in magnitude, the importance and nature of many-body effects become important.

We restrict ourselves to the case $\zeta=0$. Suppose that we use $\tau(x)$ to model a local toggling between uniform-reference-system-based DFT and the exact long-ranged limit

$$E_C^{\mathrm{LC}}[n] = \int_{-\infty}^{\infty} dx \{ f(\tau(x)) \epsilon_C^{\mathrm{LDA}}(n(x),0) - \{1 - f(\tau(x))\} \epsilon_{\mathrm{HX}}(n(x),0) \} n(x), \quad (15)$$

where, $f(\tau)=0$ if $\tau=1$ and otherwise has a value of unity for the two-fermion system, but in general, a more complicated form is necessary. We call this functional LC for *locally cognizant*, referring to the fact that the approximation is similar to the LDA but allows for the recognition and proper treatment of single-particle regions. Equation (15) produces the same LDA results for Diracium and the small-spacing double-well problem since $\tau(x)=1/2$ everywhere for these systems. For stretched 1D H_2, $\tau(x)=1$ for the exact solution. LDA gives $\tau(x)=1/2$ and the wrong energy.

To handle the large separation limit, we need to consider details about the Kohn-Sham reference system. In this limit, the highest occupied and lowest unoccupied approximate KS orbitals are nearly degenerate and it is plausible that the exact KS potential would result in orbitals that most closely resemble linear combinations of these. If we were to express the exact KS orbitals in terms of the approximate ones, we would no longer be in a variational minimum of the approximate KS system and, consequently, the orbital energy contribution would rise. Our approximate density function must then lower the interaction energy to compensate for this effect.

This LC functional will give the correct result if the interaction energy is lowered by a greater amount than the Aufbau rule raises the energy. The scheme implies that symmetry can be broken. There are two lowest-energy KS solutions: one with the up fermion localized right and the down localized left and vice versa. The total density for each is the same, but the magnetization is inverted. Since both solutions are of equal weight, the physical observables are expected to be averages of the equal-energy states. Thus, the total magnetization will vanish. The philosophy here differs from the wave-function-based idea of multiple determinants.

For example, at $a=2$, the energy change of elevating the occupied orbitals is $\Delta T_S \approx 0.037$ and the change of turning on the long-ranged part, $\Delta E_C = E_C^{\mathrm{LDA}} - E_{\mathrm{HX}} = -0.157$. These two conspire to lower the total energy. For $a=1$, the $\Delta T_S = 0.259$ dominates over $\Delta E_C = -0.195$ and the local correlation method is valid. Examination of Eq. (15) shows that LC will overcorrelate relative to the LDA but will also increase the kinetic energy. We will see later that this performance is required to improve upon the pure LDA. An optimized effective potential scheme is needed to apply LC self-consistently, even to this 1D system, and will be explored in future work.

The stretched limit poses challenges for TDDFT as well. In the large separation limit, we should have $f_{C\sigma,\tau}(x,x',\omega) = -\lambda \delta(x-x')(1-\delta_{\sigma\tau})$ because in the large separation limit $E_C = -E_{\mathrm{HX}}$. The form of Eq. (10) is compatible with this limit if $\epsilon_C = -\lambda n/4$ as the exact correlation functional should be in this limit. It would be interesting to know whether the LC LDA would correctly give this limit. This too requires an optimized effective potential scheme.

IV. METHOD OF EXACT SOLUTION

Here, we present a technique to exactly solve the eigenvalue problem $\hat{H}\psi(x_1,x_2) = E\psi(x_1,x_2)$ using $\hat{H}$ in Eq. (1). This work extends an idea originally introduced in Rosenthal's work[16] but involves many more challenges than the Diracium solution.

The exact spin-singlet real-space wave function of two 1D fermions is a two-dimensional (2D) function, $\psi(x_1,x_2)$, constrained by particle interchange rules to be either symmetric or antisymmetric under the swapping of x_1 and x_2. The eigenvalue problem is difficult to solve using the traditional wave-function-based methods of quantum chemistry such as configuration interaction because the virtual spectrum is mostly unbound. A prohibitively large number of excited configurations would be needed to provide an accurate solution. Perturbative approaches suffer similar limitations. A variational method could provide a highly accurate solution. However, the solution would be affected by the assumed form of the variational wave function. This form, in principle, limits the accuracy of the many-body solution. In this section, we present an exact numeric solution. By exact numeric, we mean an integral equation that can be solved to arbitrary accuracy numerically by increasing and refining the number of integration points.

The exact solution is found by reducing the Schrödinger equation with the Hamiltonian in Eq. (1) to a set of coupled integral equations. To do this, the differential equation is expressed in momentum space in terms of three 1D trace functions

$$G_1(k) = \int_{-\infty}^{\infty} dy \, \exp(iky)[\psi(a,y) + \psi(-a,y)], \quad (16)$$

$$G_2(k) = i\int_{-\infty}^{\infty} dy \, \exp(iky)[\psi(a,y) - \psi(-a,y)], \quad (17)$$

and

$$H(k) = \int_{-\infty}^{\infty} dy \, \exp(-iky)\psi(y,y). \quad (18)$$

Note that we use y here as the conjugate spatial coordinate to k to avoid confusion with x_1 and x_2. The k-space wave-function solution can be expressed algebraically in terms of these trace functions

$$\Phi(k_1,k_2) = \frac{2}{k_1^2 + k_2^2 + p^2}[\cos(k_1 a)G_1(k_2) + \cos(k_2 a)G_1(k_1) + \sin(k_1 a)G_2(k_2) + \sin(k_2 a)G_2(k_1) - \lambda H(k_1 + k_2)]. \quad (19)$$

The many-body energy eigenvalue is $E = -p^2/2$ defining p.

To obtain a set of 1D integral equations, we Fourier transform Eq. (19) into real space and use the result to express $\psi(a,y)$ and $\psi(-a,y)$. Then, we plug $\psi(a,y)$ and $\psi(-a,y)$ into the right-hand sides of Eqs. (16) and (17).

For S_0, the ground state, we write out the resulting coupled integral equations for G_1 and G_2 explicitly

$$G_1(ak) = \frac{2}{\pi}\left\{1 - a\frac{[1+\exp^{-2\sqrt{(ak)^2+(ap)^2}}]}{\sqrt{(ak)^2+(ap)^2}}\right\}^{-1}\int_0^\infty d(ak')$$
$$\left(\left\{\frac{2a\cos(ak)\cos(ak')}{(ak)^2+(ak')^2+(ap)^2} - \frac{2\lambda a^2}{\pi}[\kappa_{cc,1,ap,a\lambda}(-ak,-ak') + \kappa_{cc,1,ap,a\lambda}(-ak,ak')]\right\}G_1(ak')\right.$$
$$\left. - \frac{2\lambda a^2}{\pi}[\kappa_{cs,1,ap,a\lambda}(-ak,-ak') - \kappa_{cs,1,ap,a\lambda}(-ak,ak')]G_2(ak')\right) \tag{20}$$

and

$$G_2(ak) = \frac{2}{\pi}\left\{1 - a\frac{[1+\exp^{-2\sqrt{(ak)^2+(ap)^2}}]}{\sqrt{(ak)^2+(ap)^2}}\right\}^{-1}\int_0^\infty d(ak')$$
$$\left(\left\{\frac{2a\sin(ak)\sin(ak')}{(ak)^2+(ak')^2+(ap)^2} - \frac{2\lambda a^2}{\pi}[\kappa_{ss,1,ap,a\lambda}(-ak,-ak') - \kappa_{ss,1,ap,a\lambda}(-ak,ak')]\right\}G_2(ak')\right.$$
$$\left. - \frac{2\lambda a^2}{\pi}[\kappa_{sc,1,ap,a\lambda}(-ak,-ak') + \kappa_{sc,1,ap,a\lambda}(-ak,ak')]G_1(ak')\right), \tag{21}$$

with

$$\kappa_{cc,a,p,\lambda}(k,k') = \int_0^\infty dq\left(1 + \frac{\lambda}{\sqrt{q^2+2p^2}}\right)^{-1}\left[\left(\frac{\cos[a(k+q)]}{(k+q)^2+k^2+p^2}\right)\left(\frac{\cos[a(k'+q)]}{(k'+q)^2+k'^2+p^2}\right)\right.$$
$$\left. + \left(\frac{\cos[a(k-q)]}{(k-q)^2+k^2+p^2}\right)\left(\frac{\cos[a(k'-q)]}{(k'-q)^2+k'^2+p^2}\right)\right]. \tag{22}$$

We have placed prefactors of a in locations that are convenient for numerical reasons. A similar set of equations can be written down for the S_1 state. S_2 satisfies the above set with a different p. $\kappa_{cc,a,p,\lambda}(k_1,k_2)$ can be evaluated explicitly using complex analysis. The notation cc stands for the trigonometric functions that are contained in κ. cc is for cos cos, cs for cos sin, and so on. The square root introduces a branch cut affecting the contour integration that is best handled through Gauss-Legendre numerical integration.

So, we arrive at a set of coupled 1D integral equations in two functions $G_1(k)$ and $G_2(k)$. Converting the integrals to Gauss-Legendre sums allows us to express the coupled integral equations as a matrix problem

$$\begin{pmatrix} G_1 \\ G_2 \end{pmatrix} = \mu(p)\begin{pmatrix} M_{11} & M_{21} \\ M_{12} & M_{22} \end{pmatrix}\begin{pmatrix} G_1 \\ G_2 \end{pmatrix}, \tag{23}$$

where $\mu(p)$ is an eigenvalue that equals unity when the appropriate p that satisfies the original eigenvalue problem is inputted.

In expressing the integral equation in matrix form, the integrals are discretized onto a set of points. There is no unique way to do this. We chose a Gauss-Legendre inspired integration scheme. However, the implementation is not straightforward as the integrals take on the form

$$\int_0^{-\infty} dk \frac{\mathrm{trig}^2 k}{(k^2+p^2)(k^2+p^2/2)}\xi(k), \tag{24}$$

where the function $\mathrm{trig}^2 k$ can be $\cos^2 k$, $\sin^2 k$, or $\sin k \cos k$ and $\xi(k)$ is a smooth continuous function of k. To obtain accurate numerical quadratures, we break up the domain into intervals of $\pi/2$ and integrate each separately using a suitable method. For convergence to better than 10 nano-Hart, in energy and 10^{-8} in $\mu(p)$ at $a=1$, we need 800 grid points for the primary integration region and 200 additional tail points to model a portion of the asymptotic tail. The complicated scheme is highly accurate and has been verified by producing the exactly known noninteracting results to nine significant figures for 1000 k points.

Two tests verify the accuracy of the exact solution. First, the exact solution is shown to approach the known united-atom limit. The idea is that this exact solution should give results approaching Diracium's with an appropriate combined potential strength. For two wells with $Z=1$ each, we get Diracium with $Z=2$. Figure 1 shows the energy for 1D H_2 for various a and methods and the approach can be seen. The approximate methods will be discussed in Sec. V. The far left limit on the plot is Diracium when $\lambda=1$ and $Z=2$, $E_2=-3.155$. For crushed H_2, we find $E=-3.023$ when $a=0.01$ and $E=-3.087$ when $a=0.005$ extrapolating to $E_2=-3.152$ in excellent agreement with the united-atom limit.

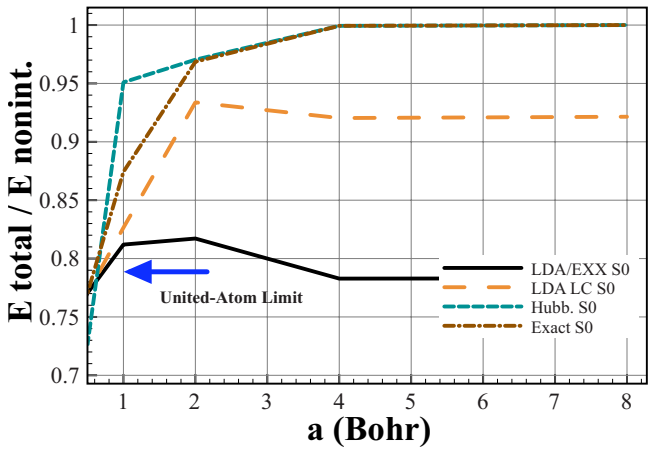

FIG. 1. (Color online) Normalized ground-state energies for the $1DH_2$ at separation a and interaction strength, $\lambda=1$, within several approximations. The results are normalized by the noninteracting result. In the asymptotic limit, the ratio should be unity. The solid line is the LDA result, the long dashed line is the LDA LC result, the medium-dashed line is the Hubbard result, the long-dashed line with diamonds is the exact result, and the arrow indicates the united-atom Diracium limit.

As a second test, the exact numeric solutions are shown to satisfy the generalized virial relationship given by Eq. (2) to within 10 μHart. The accuracy is modest due to the numeric challenge of solving the required triple integrals with the limited sampling of k points. For $Z=1$ and $\lambda=1$, the left-hand side of Eq. (2) is -318 μHart while the right-hand side is -317 μHart in less than perfect but still acceptable agreement.

V. COMPARISON OF TDDFT AND HUBBARD MODELS TO THE EXACT RESULTS

In this section, we compare adiabatic TDDFT and the Hubbard model to the exact results. To start, we make some comments about the parameter regimes chosen. This Hamiltonian, Eq. (1), offers a rich spectrum of phenomena; however, for the sake of brevity, we have restricted ourselves to a rather arbitrarily chosen parameter ranges. As mentioned, we set $Z=1$ in this section for convenience, but results for arbitrary Z can be related via scaling.

We analyze the energy spectrum of 1D H_2 versus λ for two values of a. The first case is the double-well potential with two bound fermions and separation $a=1$. In this case, we expect DFT to provide an accurate description of the spectrum since the fermions are both localized in the area of the double well. The Hubbard ground state is expected to be too low by at least 68 mHart, the amount that the kinetic energy is misrepresented in the noninteracting case. For the second case $a=2$, the system is in the stretched H_2 limit. The LDA is known to be unreliable in this limit because its failure to capture the localization of fermions to opposite sites without symmetry breaking. On the other hand, the Hubbard model is designed to work well in the stretched case. For example, the noninteracting Hubbard error at $a=2$ is less than 3 mHart for the ground state, S_0. For now, our primary focus is on comparing stable results, and thus, we restrict our analysis to $\lambda<2$, safely within the bound regime for the ground state, S_0.

Our labeling scheme for the quantum states is motivated by the noninteracting many-particle spectrum. The noninteracting multiple particle spectrum can be constructed from the single-particle states. For the two-particle solution, products of the single-particle orbitals must be properly symmetrized. The entire bound spectrum of the noninteracting two-particle states is given in Table I. Note that the nonstandard labeling of the states is used because angular momentum needed for the traditional labeling scheme is not well defined in 1D. There are three spin-singlet states and three spin-triplet states. The spin-singlet states have symmetric wave functions under particle interchange. There are two single-particle orbitals, *gerade* and *ungerade* ones, and three unique symmetric products can be made of these. The triplet state is triply degenerate in the spin manifold but has only one spatial contribution, an antisymmetrized product of the *gerade* and *ungerade* orbitals. Antisymmetric products of like noninteracting orbitals vanish. It is pointed out that the singlet state comprised of a product of two *ungerade* orbitals represents a double excitation from the ground state. The states are labeled S_0, S_1, and S_2 in the singlet manifold and T_1 in the triply degenerate triplet manifold. A transition form $S_0 \rightarrow S_1$ is the first singlet excitation, and a transition form $S_0 \rightarrow T_1$ is the first triplet excitation. Both are calculable in first-order linear-response theory of DFT. A transition form $S_0 \rightarrow S_2$ is a double excitation, proportional to the intensity of light squared, and is formally beyond first-order response theory. This fact can be realized by considering the noninteracting response function and noting that no double poles exist. Nevertheless, the bare KS double excitations might be considered a good first approximation to the double excitation due to the linear-response terms vanishing and a better approximation than the KS single excitations were to their counterparts.

The interacting two-fermion spectrum is expected to have a one-one correspondence with the noninteracting one excepting the possible disappearance of the highest energy states into the continuum as the interaction, λ, is increased. Take, for example, the 1D analog of helium, Diracium, at $Z=1$. A single δ well typically can bind two fermions of opposite spin in 1D, but above $\lambda_{\text{crit}}=2.667\,353\,225\,8$, the two-particle state merges with the continuum and only one fermion can be bound.[16,26] For two fermions in a double well, the critical interaction strength, $\lambda_{\text{crit}\,H_2}(a,S)$, depends on the well spacing, a, and state, S. The critical interaction strength, $\lambda_{\text{crit}\,H_2}(a,S)$, is likely larger than its corresponding value for a single well due to the stabilization effects of the hybridized orbitals or, in Hubbard parlance, the energetic favor ability of hopping. Most likely, each excited state in the double well has a different critical value as the higher energy states are likely to vanish at smaller λ than the ground state. However, the triplet state is interaction independent because like spins do not experience the contact interaction.

In Fig. 1, the total energies are normalized by the noninteracting results for $\lambda=1$. In the limit of large a, the ratio should become unity as the well-separated fermions will not interact but will reside on different sites. The exact solution

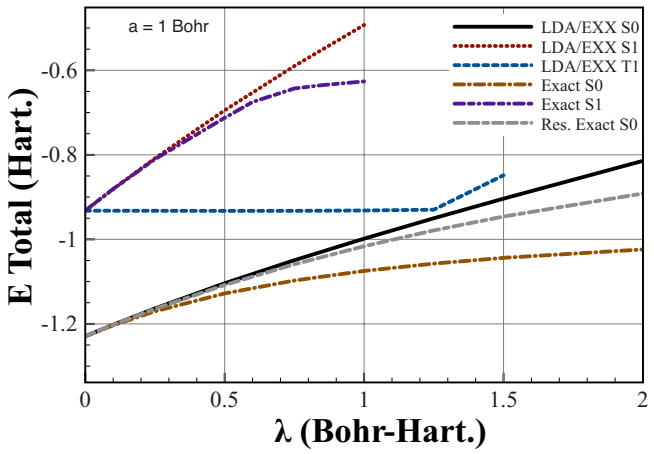

FIG. 2. (Color online) DFT and exact energy spectrum in atomic units for the $1DH_2$ for various λ with interatomic separation, $a=1$. These results are generated through the exact solution of the quantum many-body problem and the LDA version of TDDFT. S_0 and S_1 are the ground state and first singlet excited state and T_1 is the first triplet excited state. The solid line is the LDA S_0 result, the gray varyingly dashed line is a restricted version of the exact result, the long-dashed line with diamonds is the exact result for S_0, the dotted line is the LDA S_1 result, the medium-dashed line is LDA T_1 result, and the alternating short-dashed line is the exact S_1 result.

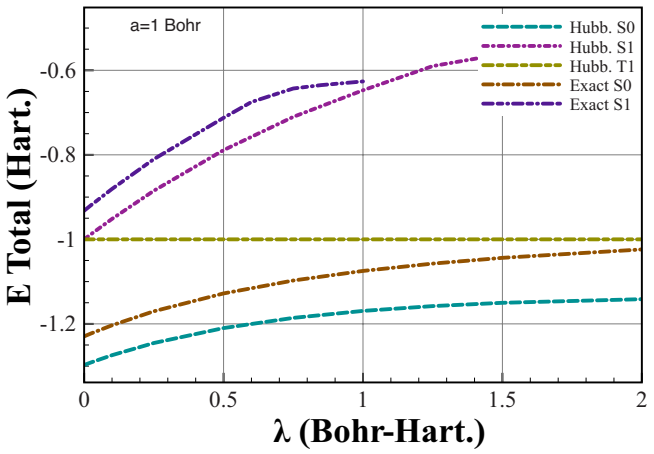

FIG. 3. (Color online) Hubbard and exact energy spectrum in atomic units for the $1DH_2$ for various λ with interatomic separation, $a=1$. The long-dashed line with diamonds is the exact result for S_0, the alternating short-dashed line is the exact S_1 result, the long-dashed line is the Hubbard S_0, the alternating short-long line is the Hubbard S_1 result, and the alternating medium-dashed line is the Hubbard T_1 result.

is globally spin unpolarized but locally acquires a nontrivial spin dependence. This is the statement that the two fermions will occupy different sites and break symmetry. The exact S_0 result here is the fully unconstrained solution of the 1D H_2 Hamiltonian. The Hubbard model S_0 reproduces the long-range charge-separated limit accurately but fails to describe the crushed limit due to improper scaling of the hoping term in this limit. This is seen through the scaling behavior of the hoping term. The LDA/EXX S_0 does approach the crushed atom limit as is expected from earlier work on the Diracium system. However, the LDA alone fails to capture long-ranged charge separation and fails to capture about 25% of the total energy in the stretched limit. A perturbative application of the LDA LC S_0 greatly improves this approach since it allows for opposite spins to become separated. In the intermediate range, $a\sim 1-2$, the DFT method and Hubbard model bracket the exact result indicating that both proper scaling and ability to localize particles are vital in this range.

In Fig. 2, we see the energy spectrum plotted for 1D H_2 with $a=1$ at various interaction strengths, λ. The exact result does not level out with increasing interaction strength. The system probably ionizes at some critical interaction strength as was the case for Diracium. Exact ground-state (exact S_0) and restricted exact ground-state (res. exact S_0) results are presented. In the latter, the solution is expressed purely in terms of $G_1(k)$ with the antisymmetric $G_2(k)$ forced to vanish [see Eqs. (20) and (21)]. In wave-function theory, this corresponds to unbroken symmetry. The result is a higher energy solution than the true broken-symmetry ground state. The difference for weak interactions is negligible but at larger interactions the restriction causes an energetic error exceeding 10% and a qualitative prediction of the cross over between the triplet excited state and the ground state. The exact result does not cross over. This finding highlights the importance of symmetry breaking in describing static correlation in the design of density functionals.

LDA/EXX S_0 and the restricted exact S_0 results are in excellent agreement until $\lambda=1$. Beyond this point the two deviate slightly but increasingly. This is most likely due to the difficulties of approaching the ionization threshold where the density is less localized. The S_1 states agree up to $\lambda=0.5$. The LDA S_1 fails to display the leveling off of the exact S_1 result. The DFT triplet (LDA/EXX T_1) results like the Hubbard (shown in Fig. 3) and exact triplets are constant. However, at $\lambda=1.2$, the triplet state becomes unreliable. This is due to the crossover between the DFT ϵ_0 energy and the ϵ_1 orbital energy. The single-pole approximation becomes numerically unstable and thus unreliable.

For the ground state, KS theory performs quite outstandingly reproducing 98% of the restricted ground-state energy at $\lambda=0.5$. In the strongly interacting regime at $\lambda=2$, DFT still gives a result within 80% of the exact value. EXX on the other hand would be more inaccurate giving about 60% of the total energy. This is worrisome because the EXX method is related to the Hartree-only theory and the nonlinear Schrödinger equation that is popular in many treatments of 1D systems. We see here an example that nonlinear Schrödinger approach does not work accurately or reliably for moderate to strong-interaction strengths. Although the DFT results perform exceptionally well up to moderate interaction strengths, the results are undercorrelated for stronger interactions, $\lambda>0.5$. This is because partial localization of the fermions to opposite ends of the system is not accounted for. The exact restricted results correspond to a solution of the integral equations with $G_2(k)$ forced to vanish. This is valid for the noninteracting solution because in that case the eigenstates are single Slater determinants of noninteracting single-particle solutions. For the interacting state, the *restricted* result does not represent a true eigenstate of the

original Hamiltonian and according to the variational principle, has a higher energy than the exact ground state. Notwithstanding, the restricted energies agree quite well with the pure LDA values indicating that LDA correlation is adequate to describe the system if there were no localization.

TDDFT allows us to find the spectrum of excited states. For the S_1 state, we show only up to $\lambda=1$ in Fig. 2. At larger interaction strengths, this state tends to be unstable and decays into an unbound Fermion and one bound Fermion. As a measure of this accuracy for TDDFT in the two-state model, we work backward. The triplet state does not experience the interaction so the triplet excitation is known exactly without using the TDDFT formalism. The triplet is unaffected by the interaction and should be a straight horizontal line with respect to λ. Thus, TDDFT should reproduce this line if the kernel and orbitals are both accurate. This is what is seen up to about $\lambda \approx 1.2$. At this point the triplet energy and the singlet-restricted ground-state energy are close hinting at a level crossing. The occurrence of a crossover differs from the Hubbard model where no level crossing occurs. The total-energy excited-state gap for the singlet is much larger than for the triplet gap. It is interesting to note that the singlet gap at $\lambda=1$ is only about one quarter larger than at $\lambda=0$. Adiabatic effects are important, but the ratio of the singlet to triplet gaps grows more than the energy of the singlet state. The actual nonadiabaticity must be a very complicated functional of the excited-state energies to capture this behavior. For the triplet to be well reproduced implies that the potential, orbitals, and kernel (at this energy range) are accurate. But the prediction of the first singlet excitation is not as accurate. Since the orbitals and potential are the same for the singlet, the approximation of the kernel must not be as accurate in the calculation of the singlet.

The Hubbard S_0 a=0 is typically overcorrelated as shown in Fig. 3. This is, in part, due to overemphasis of the kinetic energy at this smaller spacing. But the model is also qualitatively wrong for larger interactions as the energy goes to a constant while the exact result continues to grow with the interaction strength U until the system is eventually ionized. The two-site Hubbard Hamiltonian does not allow for unbound states and is consequently incapable of describing ionization. In Fig. 3, the ground-state (S_0) Hubbard curve resembles the exact curve except for a offset of about 0.1 Hartree. This lower energy is a result of the improper scaling of the kinetic-energy hopping term in the united-atom limit. The Hubbard S_1 state suffers from a similar offset problem, however, the S_1 state does not demonstrate the sharp leveling off of the exact result at $\lambda=0.6$. The higher energy Hubbard result can be rationalized by realizing that for large U, there will be significant projection of the localized solutions onto the other site thus increasing the effective overlap resulting in pair hopping. This increased delocalization is not described by the Hubbard model. The T_1 Hubbard curve is flat by construction since it does not depend on U, the interparticle interaction.

For the stretched case, we expect the Hubbard model to be essentially exact because the hopping term and single-site repulsion terms are accurate. This is in fact what is seen in Fig. 4. The remarkable agreement is not surprising as the single orbital overlaps decay exponentially and the relevant

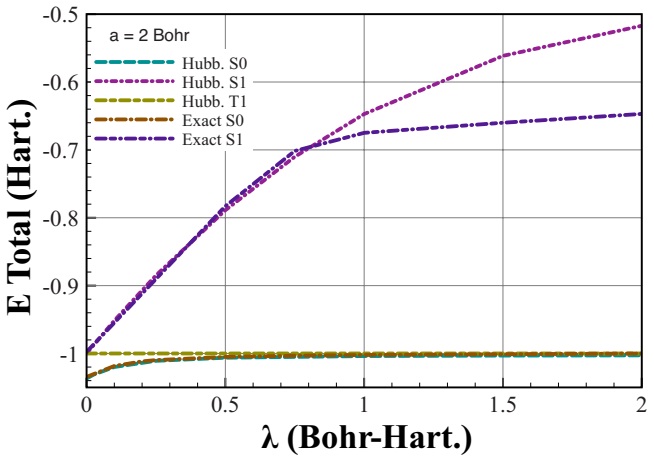

FIG. 4. (Color online) Hubbard and exact energy spectra in atomic units for the $1DH_2$ for various λ with interatomic separation, $a=2$. The long-dashed line with diamonds is the exact result for S_0, the alternating short-dashed line is the exact S_1 result, the long-dashed line is the Hubbard S_0, and the alternating short-long line is the Hubbard S_1 result.

hopping parameters are small. The T_1 Hubbard curve is again level as explained in the previous plot. For larger λ, the Hubbard result for S_1 is dangerously close to ionization ≈ -0.5. It was seen that local correlations are inadequate to properly describe ionization.

In Fig. 5, the comparison between DFT and exact is less satisfactory. The ground-state results deviate quite substantially for interactions just larger than $\lambda=0.1$. The ground-state energy is in error due to the failure of LDA to account for the localization of fermions to opposite sites. The LDA LC, applied perturbatively, does provide some of this information and thus drastically improves the agreement with the exact S_0 result. A self-consistent application of this functional would involve an optimized effective potential algo-

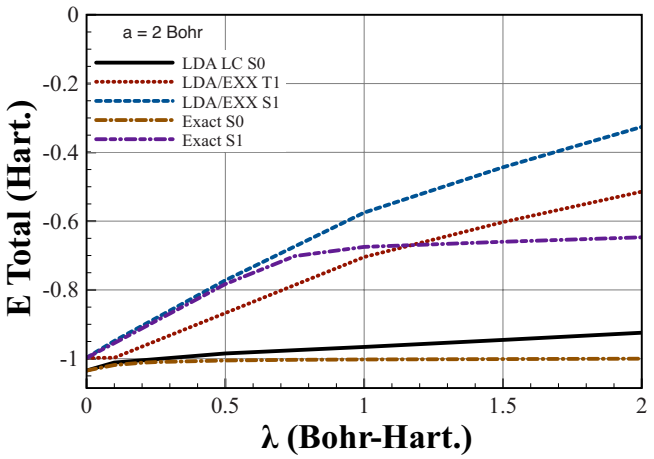

FIG. 5. (Color online) DFT and exact energy spectra in atomic units for the $1DH_2$ for various λ with interatomic separation, $a=2$. The long-dashed line with diamonds is the exact result for S_0, the alternating short-dashed line is the exact S_1 result, the dotted line is LDA LC S_0 result, the solid line is the LDA S_1 result, and the medium dashed line is the LDA T_1 result.

rithm that is beyond the scope of this work. However, self-consistency is likely to improve the accuracy. It would be interesting to find out how a TDDFT kernel based on this improved functional would perform. The perturbative approach only approximates the stretched H_2 limit while a fully self-consistent approach should exactly match at large λ. LDA/EXX T_1 only agrees up to $\lambda=0.1$. The orbitals are not faithful representations of the exact KS orbitals since the LDA ground state is inaccurate. Curiously, the LDA/EXX S_1 and exact S_1 agree exceptionally well up to $\lambda=1/2$. This is because the local kernel cancels the self-interaction correlation error in the ground-state calculation. No excited-state results are reported for LDA LC TDDFT because the method had been applied perturbatively and the self-consistent wave functions and kernel are not available in the analysis.

VI. CONCLUSION

In this paper, we have explored how two standard viewpoints of condensed-matter physics describe an interacting 1D many-particle system. One method, LDA DFT, provides accurate energies within about 0.1 mHartree for intermediate interaction strengths ($\lambda \leq 0.5$) and distances ($a<2$) but fails appreciably at large well spacings. Analysis of the exact solution shows that this limitation is due to symmetries induced by the short-sightedness of the restricted KS scheme within the LDA. When the restricted symmetry is enforced on the exact solution, the result lies much more closely to the LDA indicating that the lack of localization is the key deficiency in the restricted LDA KS treatment. To overcome this challenge, a local parameter, $\tau(x)$, is used that describes the effective local number of fermions and is readily implementable in existing electronic structure codes. This local measure allows the use of two reference systems in the construction of a density functional: the uniform-reference system and the single-particle system. The functional, when applied perturbatively, is shown to better reproduce the energy curve of 1D H_2 versus well spacing. A self-consistent application will require an optimized effective potential approach beyond the scope of this work but is likely to improve the agreement.

On the other hand, the two-site Hubbard model provides a qualitatively accurate description of the ground state across a wide range of parameters describing both united-atom and separate-atom limits, but it fails in its quantitative predictions and has questionable scaling characteristics. This is not surprising as the model is limited by design. The two-site Hubbard model does not include the continuum and will therefore fail to describe ionization and scattering.

The excited-state results follow a similar pattern as the ground-state results. DFT is accurate for small well spacings and the Hubbard model is more reliable for larger spacings. In TDDFT, the approximation of the first singlet excitation fails for weaker interactions than the lower energy triplet. For the triplet to be well reproduced implies that the potential, orbitals, and kernel (at this energy range) are accurate. Since the first two are the same for the singlet, the approximation of the kernel must not be as accurate in the calculation of the singlet. A strongly nonadiabatic kernel would explain why TDDFT predicts the lower energy triplet but not the higher energy singlet. Thus, nonadiabaticity outweighs ultranonlocality problems. Perhaps, this is due to the locality of exchange for contact interactions and could be quite different from what occurs with long-ranged 3D interactions. Curiously, the Hubbard first-excited state can also prove drastically wrong in cases when the fermions are strongly interacting, large U, as the Hubbard treatment forces same site localization while the exact system will have significant pair delocalization. This result has significant implications for the reliability of LDA+U results with large U.

The realm of 1D contact-interacting fermions provides an interesting opportunity to compare the Hubbard and DFT models in detail. Results found here provide insight into models of 3D Coulomb interacting systems where many of the underlying quantum many-body effects are obfuscated by the long-ranged nature of the interaction.

APPENDIX A

In this appendix, we find the third-order λ term in the high-density limit of the correlation energy per particle for Deltium, the one-dimensional uniform fermion system, using the Goldstone diagrammatic approach to perturbation theory in momentum space.[27]

The Fourier transform of the interaction potential is $V(q)=\frac{\lambda}{L}\int_{-L}^{L}dx\,\delta(x)e^{iqx}=\frac{\lambda}{L}$, where L is the arbitrary length between the boundaries confining the system. Like spin fermions do not interact via the δ function; this means that only vertices that connect opposite spins enter into the diagrammatic series. This is a tremendous simplification as many diagrams vanish. A further simplification is that the interaction is independent of the momentum transfer, q.

To third order, three different diagrams contribute as seen in Fig. 6. The momenta in each diagram are labeled according to the arrows in the two-bubble diagram shown in Fig. 7. From the standard rules of perturbation theory, the third-order term can be written as a sum of multidimensional integrals

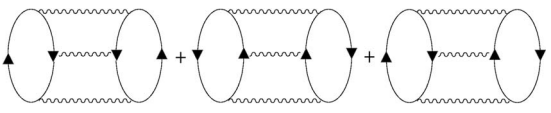

FIG. 6. Diagrammatic representation of the third-order contributions to the interaction energy. Spin labels are omitted since the two loops in each diagram must have opposite spins. Up arrows represent particles and down arrows represent holes. The final diagram contributes twice because a horizontal rotation produces a new diagram.

$$N\epsilon_C^{(3)} = \frac{\lambda^3}{L^3}\frac{L^4}{16\pi^4}\frac{n_s}{2}\left(\int_{-\infty}^{\infty}dq\int_{-\infty}^{\infty}dr\int_{k_F}^{\infty}d|k_1|\int_{k_F}^{\infty}d|k_2|\frac{1}{q(q+k_1-k_2)r(r+k_1-k_2)}\right.$$
$$\left.+\int_{-\infty}^{\infty}dq\int_{-\infty}^{\infty}dr\int_{-k_F}^{k_F}dk_1\int_{-k_F}^{k_F}dk_2\frac{1}{q(q+k_1-k_2)r(r+k_1-k_2)}-2\int_{-\infty}^{\infty}dq\int_{-\infty}^{\infty}dr\int_{k_F}^{\infty}d|k_1|\int_{-k_F}^{k_F}dk_2\frac{1}{qr(k_1+k_2)^2}\right), \quad \text{(A1)}$$

with $|k_1+q|>k_F$, $|k_1+r|>0$, $|k_2-q|>k_F$, and $|k_2-r|>0$ for the first term, with $|k_1+q|<k_F$, $|k_1+r|<0$, $|k_2-q|<k_F$, and $|k_2-r|<0$ for the second term, and with $|k_1+q|<k_F$, $|k_1+r|<0$, $|k_2-q|>k_F$, and $|k_2-r|>0$ for the final term. The notation $\int_{k_F}^{\infty}d|k|$ stands for the sum of two integrals, $\int_{k_F}^{\infty}dk+\int_{-\infty}^{-k_F}dk$. k_1 and k_2 are particle (or hole) momenta and q and r are the momentum transfers. n_s is the number of spin species, in this case 2. The limits of integration and constraint inequalities ensure that particles have less momentum than the Fermi momentum and holes have higher momentum than the Fermi momentum. There is a symmetry factor of 1/2 associated with each diagram. The third diagram contributes twice because a horizontal rotation produces a new diagram with the same numerical value. This third diagram contributes a negative value because an odd number of vertices connects particle to holes. To integrate Eq. (A1) exactly, we rescale as follows: $q=k_F v$, $r=k_F x$, $k_1=k_F y$, and $k_2=k_F z$. The correlation energy per particle in third order in λ is found to be

$$\epsilon_C^{(3)} = \frac{\lambda^3}{16\pi^4}\left(\frac{L}{N}\right)(\mathcal{I}_a+\mathcal{I}_b-2\mathcal{I}_c) = \frac{\zeta(3)}{2\pi^4}\frac{\lambda^3}{n} \quad \text{(A2)}$$

using the quadrature results

$$\mathcal{I}_a = 2\int_2^{\infty}dv\int_2^{\infty}dx\int_{-1}^{1}dy\int_{-1}^{1}dz\frac{1}{vx(v+y-z)(x+y-z)}$$
$$+2\int_2^{\infty}dv\int_{-\infty}^{-2}dx\int_{-1}^{1}dy\int_{-1}^{1}dz\frac{1}{vx(v+y-z)(x+y-z)}$$
$$+4\int_0^{2}dv\int_0^{v}dx\int_{1-x}^{1}dy\int_{-1}^{-1+x}dz\frac{1}{vx(v+y-z)(x+y-z)}$$
$$+2\int_0^{2}dv\int_{2-v}^{2}dx\int_{1-v}^{x-1}dy\int_{1-x}^{v-1}dz\frac{1}{vx(v+y-z)(x-y+z)}$$
$$+4\int_2^{\infty}dv\int_0^{2}dx\int_{1-x}^{1}dy\int_{-1}^{-1+x}dz\frac{1}{vx(v+y-z)(x+y-z)}$$
$$+4\int_2^{\infty}dv\int_{-2}^{0}dx\int_{-1-x}^{-1}dy\int_{1+x}^{1}dz\frac{1}{vx(v+y-z)(x+y-z)}$$
$$=8\pi^2\ln 2-36\zeta(3), \quad \text{(A3)}$$

$$\mathcal{I}_b = 4\int_2^{\infty}dv\int_{v-2}^{v}dx\int_{v-1}^{1+x}dy\int_{v-1}^{1+x}dz\frac{1}{vx(y+z-v)(y+z-x)}$$
$$+4\int_0^{2}dv\int_0^{v}dx\int_1^{1+x}dy\int_1^{1+x}dz\frac{1}{vx(y+z-v)(y+z-x)}$$
$$=-8\pi^2\ln 2+48\zeta(3), \quad \text{(A4)}$$

and

$$\mathcal{I}_c = 4\int_0^{2}dv\int_0^{v}dx\int_1^{1+x}dy\int_{1-x}^{1}dz\frac{1}{vx(y+z)^2}$$
$$+4\int_2^{4}dv\int_2^{v}dx\int_{v-1}^{1+x}dy\int_{-1}^{1}dz\frac{1}{vx(y+z)^2}$$
$$+4\int_2^{4}dv\int_{v-2}^{v}dx\int_{v-1}^{1+x}dy\int_{1-x}^{1}dz\frac{1}{vx(y+z)^2}$$
$$+4\int_4^{\infty}dv\int_{v-2}^{v}dx\int_{v-1}^{1+x}dy\int_{-1}^{1}dz\frac{1}{vx(y+z)^2}=2\zeta(3). \quad \text{(A5)}$$

The author suspects that an even more tedious calculation reveals that the correlation energy per particle to fourth order in λ is

$$\epsilon_C^{(4)} = -\frac{3\zeta(3)}{4\pi^6}\frac{\lambda^4}{n^2} = -0.000\,938\frac{\lambda^4}{n^2}. \quad \text{(A6)}$$

This value agrees well with the numeric Bethe-Ansatz result of $-0.000\,94\lambda^4/n^2$. The full derivation will be given in a later work.

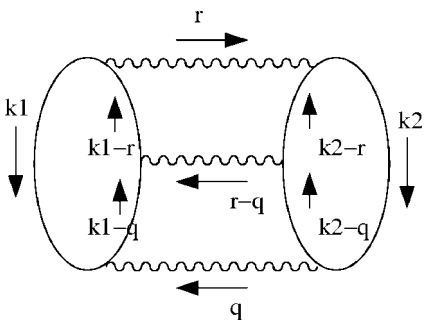

FIG. 7. Momentum labels for the third-order contributions to the interaction energy. q and r are momentum transfers. k_1 and k_2 can label particle or hole momenta depending on the diagram.

APPENDIX B

In the (4,4) Padé parameterization of $\epsilon_{\mathrm{XC}}(n,\zeta)$, we have used the result that there exists an astonishing nonlinear analytic relationship between the given expansion limits and the desired Padé parameters. A (4,4) Padé of the form

$$F(x) = \frac{Ax^4 + Bx^3 + Cx^2}{Dx^3 + Ex^2 + Fx + 1} \tag{B1}$$

has parameters A, B, C, D, E, and F chosen to satisfy known limits. If three terms in both the large and small x limits are known as given below, we can fit these parameters exactly. Specifically, if for large x,

$$F(x) = g_1 x + g_2 + g_3/x + \cdots, \tag{B2}$$

and if, for small x,

$$F(x) = g_4 x^2 + g_5 x^3 + g_6 x^4 + \cdots. \tag{B3}$$

The parameters A-F can be determined explicitly.

Let us introduce the following nonlinear Ansatz for the parameters:

$$A = \frac{g_1(g_4^3 + 2g_1g_5g_4 + g_2g_6g_4 - g_2g_5^2 + g_1^2g_6)}{g_1^3 + 2g_2g_4g_1 + g_3g_5g_1 + g_3g_4^2 - g_2^2g_5}, \tag{B4}$$

$$B = \frac{g_5g_1^3 + g_4^2g_1^2}{g_1^3 + 2g_2g_4g_1 + g_3g_5g_1 + g_3g_4^2 - g_2^2g_5} + \frac{[g_2g_4g_5 + g_3(g_5^2 - g_4g_6)]g_1 + g_2(g_4^3 + g_2g_6g_4 - g_2g_5^2)}{g_1^3 + 2g_2g_4g_1 + g_3g_5g_1 + g_3g_4^2 - g_2^2g_5}, \tag{B5}$$

$$C = g_4, \tag{B6}$$

$$D = A/g_1, \tag{B7}$$

$$E = \frac{g_5g_1^2 + g_4^2g_1 - g_2g_6g_1 + g_3g_5^2 - g_2g_4g_5 - g_3g_4g_6}{g_1^3 + 2g_2g_4g_1 + g_3g_5g_1 + g_3g_4^2 - g_2^2g_5}, \tag{B8}$$

and

$$F = \frac{g_4g_1^2 - (g_2g_5 + g_3g_6)g_1 + g_2g_4^2 - g_3g_4g_5 + g_2^2g_6}{g_1^3 + 2g_2g_4g_1 + g_3g_5g_1 + g_3g_4^2 - g_2^2g_5}, \tag{B9}$$

Direct substitution of Eqs. (B4)–(B9) into the Eq. (B1) gives the desired high and low-density expansions, Eqs. (B2) and (B3).

APPENDIX C

The exact spin dependence of the exchange-correlation energy was alluded to in the body of the paper. Here, we present the exact result in the high-density limit. For completeness, recall that the spin-dependent Hartree and exchange energy per particle is

$$\epsilon_{\mathrm{HX}}(n_\uparrow, n_\downarrow) = \lambda n_\uparrow n_\downarrow/(n_\uparrow + n_\downarrow).$$

In the high-density limit, correlation energy contributes to second order in λ. This contribution is described by the two-bubble diagram shown second in Fig. 7 of Ref. 4. From the standard rules of perturbation theory, the diagram can be expressed as an integral

$$N\epsilon_C^{(2)}(n_\uparrow, n_\downarrow) = -\frac{\lambda^2}{L^2}\frac{L^3}{8\pi^3}\int_{-\infty}^{\infty} dq \int_{-k_{F\downarrow}}^{k_{F\downarrow}} dk_1 \int_{-k_{F\uparrow}}^{k_{F\uparrow}} dk_2 \times \frac{1}{q(q + k_1 - k_2)},$$

with $k_{F\uparrow} = n_\uparrow/2$, $k_{F\downarrow} = n_\downarrow/2$, $|k_1 + q| > k_{F\uparrow}$, and $|k_2 - q| > k_{F\downarrow}$, where k_1 and k_2 are particle momenta and q is the momentum transfer. Once again the symmetry factor of 1/2 is canceled by the two possible spin configurations. To solve Eq. (B1) exactly, we define two quantities k_F and s according to the following: $k_{F\uparrow} = k_F(1-s)$ and $k_{F\downarrow} = k_F s$. Then, we rescale the coordinates as follows: $q = k_F x$, $k_1 = k_F y$, and $k_2 = k_F z$. Note that $s = n_\downarrow/n$ and $\zeta = 1 - 2s$. After some algebra, we find the correlation energy per particle

$$\begin{aligned}\epsilon_C^{(2)} &= -\frac{\lambda^2}{8\pi^3}\left(\frac{L}{N}\right)\frac{\pi}{2} n\mathcal{I}(\zeta) \\ &= -\frac{\lambda^2}{24} f(\zeta) \\ &= -\frac{\lambda^2}{4\pi^2}\left(\frac{\pi^2}{2} - (1-\zeta)\Re\mathrm{Di}\ \mathrm{Log}(1-\zeta) - (1+\zeta)\Re\mathrm{Di}\ \mathrm{Log}(1+\zeta)\right)\end{aligned}$$

using the quadrature result below and replacing s by $1/2(1-\zeta)$,

$$\begin{aligned}\mathcal{I}(s) &= \int_{2-2s}^{\infty} dx \int_{-s}^{s} dy \int_{s-1}^{1-s} dz \frac{1}{x(x+y-z)} \\ &\quad + \int_{0}^{2s} dx \int_{s-x}^{s} dy \int_{s-1}^{x+s-1} dz \frac{1}{x(x+y-z)} \\ &\quad + \int_{2s}^{2-2s} dx \int_{-s}^{s} dy \int_{s-1}^{x+s-1} dz \frac{1}{x(x+y-z)} \\ &= 4\left(\frac{\pi^2}{2} - (2-2s)\Re\mathrm{Di}\ \mathrm{Log}(2-2s) - 2s\Re\mathrm{Di}\ \mathrm{Log}(2s)\right).\end{aligned}$$

The approximation, $f(\zeta) \approx (1-\zeta^2)$, is only true for the extreme values of ζ with relative errors of up to about 33.333%. An expansion of ϵ_C about $\zeta = 0$, for example, reveals logarithmic dependencies. In the small ζ, nearly unpolarized limit,

$$f(\zeta) = 1 - \frac{9}{\pi^2}\zeta^2 + \frac{6}{\pi^2}\zeta^2 \log \zeta + \mathcal{O}(\zeta^3). \tag{C1}$$

Perhaps this interesting behavior has implications for the effects of correlation on 1D spin-density waves and this will be

TABLE II. Sample exact-exchange DFT results through the solution of Eq. (D1) for $a=1$ and $Z=1$.

λ	ϵ	m	M	x_0
0.0	0.61478	1.0	∞	∞
0.00689	0.61459	0.999	13.3504	3.6267
0.6266	0.44646	0.9	1.19376	1.31123
1.183	0.31075	0.8	0.72483	0.93000
1.721	0.19480	0.7	0.47586	0.67034
2.295	0.9239	0.6	0.28378	0.43249
2.640	0.04511	0.55	0.18487	0.29433
3.040	0.00886	0.51	0.07634	0.12800

explored further in latter work. Likewise, expansion about $\zeta=1$ shows

$$f(\zeta) = \frac{6}{\pi^2}(\zeta - 1)\,\Re\mathrm{Di}\,\mathrm{Log}(2). \tag{C2}$$

APPENDIX D

The problem in Eq. (1) can be solved analytically within the restricted exact-exchange density-functional approach. For the ground state, the solution is spin unpolarized. The relevant KS equation for one spin-wave-function is

$$-\frac{1}{2}\nabla^2\phi(x) + \lambda|\phi(x)|^2\phi(x) - Z\sum_{\pm}\delta(x \pm a)\phi(x) = -\epsilon\phi(x). \tag{D1}$$

This is the nonlinear Schrödinger equation in a double-well potential. For simplicity, we only present results for $a=1$. The solution, vanishing at a distance, can be shown analytically to be

$$\phi(x) = \begin{cases} \sqrt{\dfrac{1-m}{2m-1}}M\ \mathrm{JacobiNC}\left(\sqrt{\dfrac{2\epsilon}{2m-1}}x, m\right) & |x| < 1 \\ M\ \mathrm{csch}(\sqrt{2\epsilon}(|x|-1) + x_0) & |x| > 1, \end{cases} \tag{D2}$$

where JacobiNC is a Jacobi elliptic function. The wave-function is continuous at x=1. The double-well potential forces cusps at the ± 1. The constraint can be expressed as a transcendental equation. The other constraint is that the wave function must normalized to unity. These two are solved numerically simultaneously. We present some representative numeric solutions in Table II. These values and others were used in the paper to validate the LDA code.

*Current address: Sandia National Laboratories, Albuquerque, New Mexico 87185–1322, USA.

[1] J. K. Chin, D. E. Miller, Y. Liu, C. Stan, W. Setiawan, C. Sanner, K. Xu, and W. Ketterle, Nature (London) **443**, 961 (2006).
[2] T. Stoferle, H. Moritz, K. Gunter, M. Kohl, and T. Esslinger, Phys. Rev. Lett. **96**, 030401 (2006).
[3] H. Moritz, T. Stoferle, K. Guenter, M. Kohl, and T. Esslinger, Phys. Rev. Lett. **94**, 210401 (2005).
[4] R. J. Magyar and Kieron Burke, Phys. Rev. A **70**, 032508 (2004).
[5] G. Xianlong, M. Polini, R. Asgari, and M. P. Tosi, Phys. Rev. A **73**, 033609 (2006).
[6] Y. E. Kim and A. L. Zubarev, Phys. Rev. A **70**, 033612 (2004).
[7] G. E. Astrakharchik, D. Blume, S. Giorgini, and L. P. Pitaevskii, Phys. Rev. Lett. **93**, 050402 (2004).
[8] R. Benguria, R. Bummelhuis, P. Duclos, S. Perez-Oyarzun, and P. Vytras, Few-Body Syst. **38**, 133 (2006).
[9] M. M. Fogler, Phys. Rev. Lett. **94**, 056405 (2005).
[10] N. A. Nguyen and A. D. Bandrauk, Phys. Rev. A **73**, 032708 (2006).
[11] A. Gold, Phys. Rev. B **55**, 9470 (1997).
[12] R. J. Magyar and K. Burke (unpublished) http://chem.ps.uci.edu/~kieron/dft/book/gamma/g1.pdf
[13] V. I. Anisimov, F. Aryasetiawan, and A. I. Lichtenstein, J. Phys.: Condens. Matter **9**, 767 (1997).
[14] S. Y. Savrasov and G. Kotliar, Phys. Rev. Lett. **84**, 3670 (2000).
[15] P. Ziesche, O. Gunnarsson, W. John, and H. Beck, Phys. Rev. B **55**, 10270 (1997).
[16] C. Rosenthal, J. Chem. Phys. **55**, 2474 (1971).
[17] P. Hohenberg and W. Kohn, Phys. Rev. **136**, B864 (1964).
[18] W. Kohn and L. J. Sham, Phys. Rev. **140**, A1133 (1965).
[19] M. Gaudin, Phys. Lett. **24A**, 55 (1967).
[20] C. N. Yang, Phys. Rev. Lett. **19**, 1312 (1967).
[21] W. I. Friesen and B. Bergersen, J. Phys. C **13**, 6627 (1980).
[22] A. Recati, P. O. Fedichev, W. Zwerger, and R. P. Zoller, J. Opt. B: Quantum Semiclassical Opt. **5**, S55 (2003).
[23] E. Runge and E. K. U. Gross, Phys. Rev. Lett. **52**, 997 (1984).
[24] M. E. Casida, in *Recent Advances in Density Functional Methods, Part I*, edited by Ed Chong (World Scientific, Singapore, 1995), p. 155.
[25] J. P. Perdew, A. Savin, and K. Burke, Phys. Rev. A **51**, 4531 (1995).
[26] H. D. Cornean, P. Duclos, and B. Ricaud, Few-Body Syst. **38**, 125 (2006).
[27] J. Goldstone, Proc. R. Soc. London, Ser. A **239**, 267 (1957).